Rapid Communications

Universal gapless Dirac cone and tunable topological states in $(MnBi_2Te_4)_m(Bi_2Te_3)_n$ heterostructures

Yong Hu,[1,*] Lixuan Xu,[2,*] Mengzhu Shi,[1,*] Aiyun Luo,[3,*] Shuting Peng,[1] Z. Y. Wang,[1] J. J. Ying,[1] T. Wu,[1] Z. K. Liu,[2] C. F. Zhang,[2,4] Y. L. Chen,[2,5] G. Xu,[3] X.-H. Chen,[1,†] and J.-F. He[1,†]

[1]*Hefei National Laboratory for Physical Sciences at the Microscale, Department of Physics and CAS Key Laboratory of Strongly-coupled Quantum Matter Physics, University of Science and Technology of China, Hefei, Anhui 230026, China*

[2]*School of Physical Science and Technology and ShanghaiTech Laboratory for Topological Physics, ShanghaiTech University, Shanghai 201210, China*

[3]*Wuhan National High Magnetic Field Center and School of Physics, Huazhong University of Science and Technology, Wuhan 430074, China*

[4]*College of Advanced Interdisciplinary Studies, National University of Defense Technology, Changsha 410073, China*

[5]*Department of Physics, University of Oxford, Oxford OX1 3PU, United Kingdom*

(Received 17 December 2019; accepted 18 March 2020; published 23 April 2020)

The newly discovered magnetic topological insulators $(MnBi_2Te_4)_m(Bi_2Te_3)_n$ are predicted to be a versatile platform for exploring novel topological states. Here, we report angle-resolved photoemission spectroscopy studies on a series of $(MnBi_2Te_4)_m(Bi_2Te_3)_n$ heterostructures. An unexpected but universal gapless Dirac cone is observed on the $(MnBi_2Te_4)$ terminated (0001) surfaces in all systems, indicating an altered magnetic structure near the surface. The specific band dispersion of the surface states, presumably dominated by the top surface, is found to be sensitive to different stackings of the underlying $MnBi_2Te_4$ and Bi_2Te_3 layers. Our results suggest the high tunability of both magnetic and electronic structures of the topological surface states in $(MnBi_2Te_4)_m(Bi_2Te_3)_n$ heterostructures, which is essential in realizing and manipulating various topological states.

DOI: 10.1103/PhysRevB.101.161113

Topological materials with intrinsic magnetic orders are believed to be an ideal platform to explore and manipulate exotic topological quantum states [1–9]. This idea has been recently realized in a stoichiometric magnetic topological insulator $MnBi_2Te_4$ [10–20]. The inherent antiferromagnetic order is predicted to induce gapped surface states, which can host an exotic axion insulator state with a topological magnetoelectric effect (TME) [Fig. 1(a)] [11,12]. Recent transport results further indicate that the axion insulator state can be transformed into a Chern insulator state with the quantized anomalous Hall effect (QAHE) by tuning the magnetic structure into ferromagnetism under an external field [Fig. 1(a)] [18–20]. However, unexpected gapless topological surface states (TSSs) are observed by high-resolution angle-resolved photoemission spectroscopy (ARPES) measurements [21–24], raising critical questions regarding the surface magnetic structure, magnetic coupling strength, and the specifics of the $MnBi_2Te_4$ material system.

$(MnBi_2Te_4)_m(Bi_2Te_3)_n$ heterostructures represent a closely related but more complex system, in which both $MnBi_2Te_4$ and Bi_2Te_3 layers are essential building blocks [Figs. 1(b) and 1(c)] [10,11,25–29]. The reduced interlayer antiferromagnetic exchange coupling (due to the nonmagnetic Bi_2Te_3 layers) facilitates the magnetic manipulation [27–29], and two distinct building blocks provide an additional knob to tune the topological states by different stackings of the van der Waals layers [Figs. 1(b) and 1(c)]. In this sense, $(MnBi_2Te_4)_m(Bi_2Te_3)_n$ heterostructures are predicted to be a more versatile playground for realizing exotic topological states and topological phase transitions [27–29].

In this Rapid Communication, we report ARPES studies on a series of $(MnBi_2Te_4)_m(Bi_2Te_3)_n$ heterostructures, including $MnBi_2Te_4$ (for simplicity, we combine $MnBi_2Te_4$ into the heterostructures and mark it as $m = 1$, $n = 0$, hereafter), $MnBi_4Te_7$ ($m = 1, n = 1$), and $MnBi_6Te_{10}$ ($m = 1, n = 2$). A gapless Dirac cone is observed on the $(MnBi_2Te_4)$ terminated (0001) surfaces in all systems, demonstrating a universal gapless surface state in the $(MnBi_2Te_4)_m(Bi_2Te_3)_n$ family. This is in sharp contrast to the expected gap from the original antiferromagnetic ground state [11–13,18,30–32], but consistent with an altered magnetic structure on the cleaved $MnBi_2Te_4$ surface, echoing the tunability of the magnetic structure in the system. The band dispersions of the TSSs are also examined in these heterostructures. Different from the surface states in typical van der Waals topological insulators, whose band dispersions are mainly determined by the surface layer itself [33,34], the surface states in $(MnBi_2Te_4)_m(Bi_2Te_3)_n$ are found to be sensitive to different stackings of the underlying $MnBi_2Te_4$ and Bi_2Te_3 layers. Such behavior, when combined with a tunable magnetic structure, provides an experimental basis for the theoretical proposal to realize exotic topological states by manipulating the magnetic structure and different combinations of the two building block layers in $(MnBi_2Te_4)_m(Bi_2Te_3)_n$ heterostructures [29,35].

*These authors contributed equally to this work.

†Correspondence and requests for materials should be addressed to chenxh@ustc.edu.cn; jfhe@ustc.edu.cn

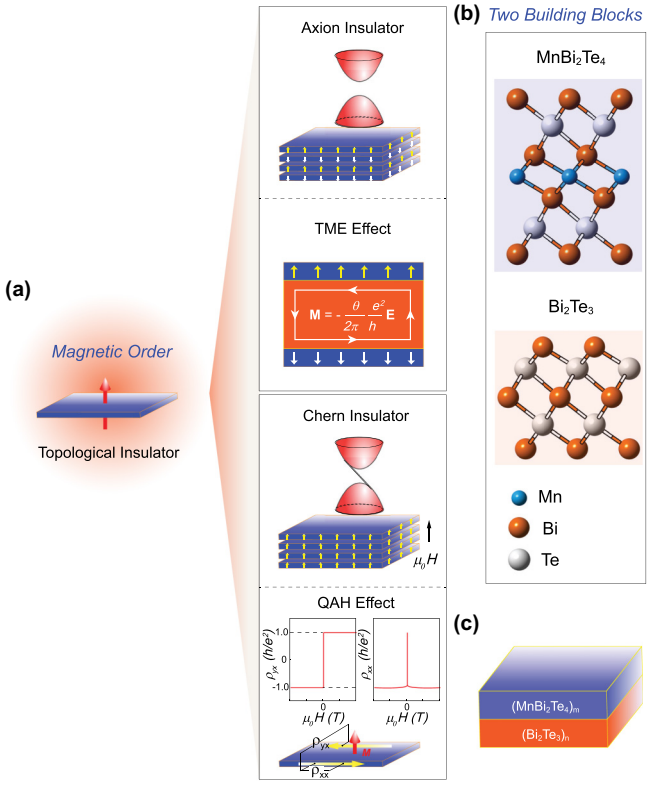

FIG. 1. Schematics of the magnetic configurations and crystal building blocks in $(MnBi_2Te_4)_m(Bi_2Te_3)_n$ heterostructures. (a) Schematic antiferromagnetic order of the axion insulator state [4] and ferromagnetic order of the Chern insulator state [3]. (b) Two crystal building blocks of the $(MnBi_2Te_4)_m(Bi_2Te_3)_n$ heterostructures. (c) Different stackings of the two building blocks give rise to different materials of the $(MnBi_2Te_4)_m(Bi_2Te_3)_n$ heterostructures.

Single crystals of $MnBi_2Te_4$, $MnBi_4Te_7$, and $MnBi_6Te_{10}$ were grown via a solid-state reaction method as described in an earlier study [14,36]. X-ray diffraction measurements were carried out on each sample to identify the correct phase (see Fig. S1 in the Supplemental Material [37]). ARPES measurements were carried out on a laser-based ARPES system with a photon energy of 6.994 eV. A small beam spot ($\sim$20 μm) was achieved and used to resolve different terminations in the real space of the sample surface. The size of each domain was estimated to be a few tens of microns. The samples were cleaved at 30 K in ultrahigh vacuum. A total energy resolution of $\sim$3 meV was used for the measurements. The base pressure was better than 3×10^{-11} mbar.

When the as-grown single-crystalline heterostructures are cleaved for ARPES measurements, different terminations are expected due to the similar strength of the van der Waals bonds in the material. By using a small beam spot, we have resolved different terminations on the cleaved sample surface and probed their electronic structures, respectively. In $MnBi_6Te_{10}$, three types of electronic structures are identified (Fig. 2), as evidenced by three sets of constant energy maps [Figs. 2(b), 2(e), and 2(h)] and electron bands [Figs. 2(c), 2(f), and 2(i)]. This is consistent with the three possible terminations of the $MnBi_6Te_{10}$ system [Figs. 2(a), 2(d), and 2(g)]. The same is true for the $MnBi_4Te_7$ ($MnBi_2Te_4$) system, in which two (one) types of electronic structures are found [Fig. S2 [37] and Figs. 3(a)–3(d); see Fig. S3 for the identification of the electronic structures on different terminations [37]].

We first focus on the $(MnBi_2Te_4)$ termination, which is the essential magnetic building block of all $(MnBi_2Te_4)_m(Bi_2Te_3)_n$ heterostructures. Comparative measurements have been carried out on the $(MnBi_2Te_4)$ termination of $MnBi_2Te_4$, $MnBi_4Te_7$, and $MnBi_6Te_{10}$ systems below their magnetic transition temperatures, respectively (Fig. 3). A Dirac-like TSS is observed around the Γ point of all three

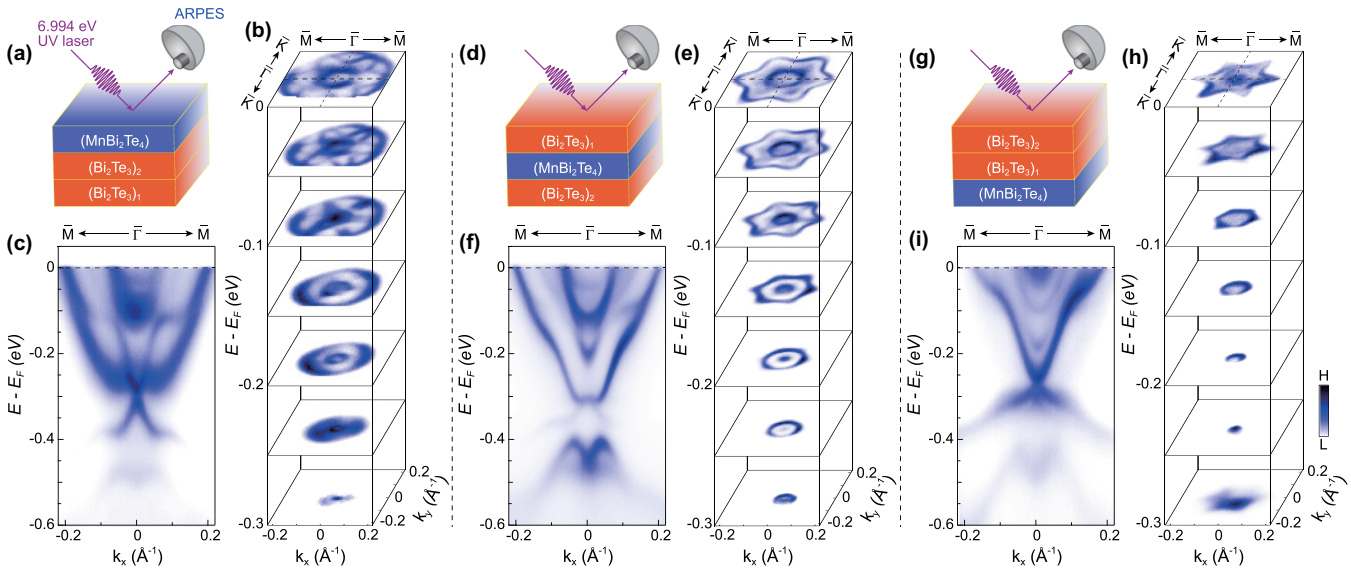

FIG. 2. Electronic structure on different surface terminations of $MnBi_6Te_{10}$. (a) Schematic of the $(MnBi_2Te_4)$ termination, (b) the corresponding constant energy maps, and (c) band dispersion along the M-Γ-M high-symmetry cut, measured at 6 K. (d)–(f) Same as (a)–(c), but for the type-1 (Bi_2Te_3) termination as illustrated in (d). (g)–(i) Same as (a)–(c), but for the type-2 (Bi_2Te_3) termination as illustrated in (g).

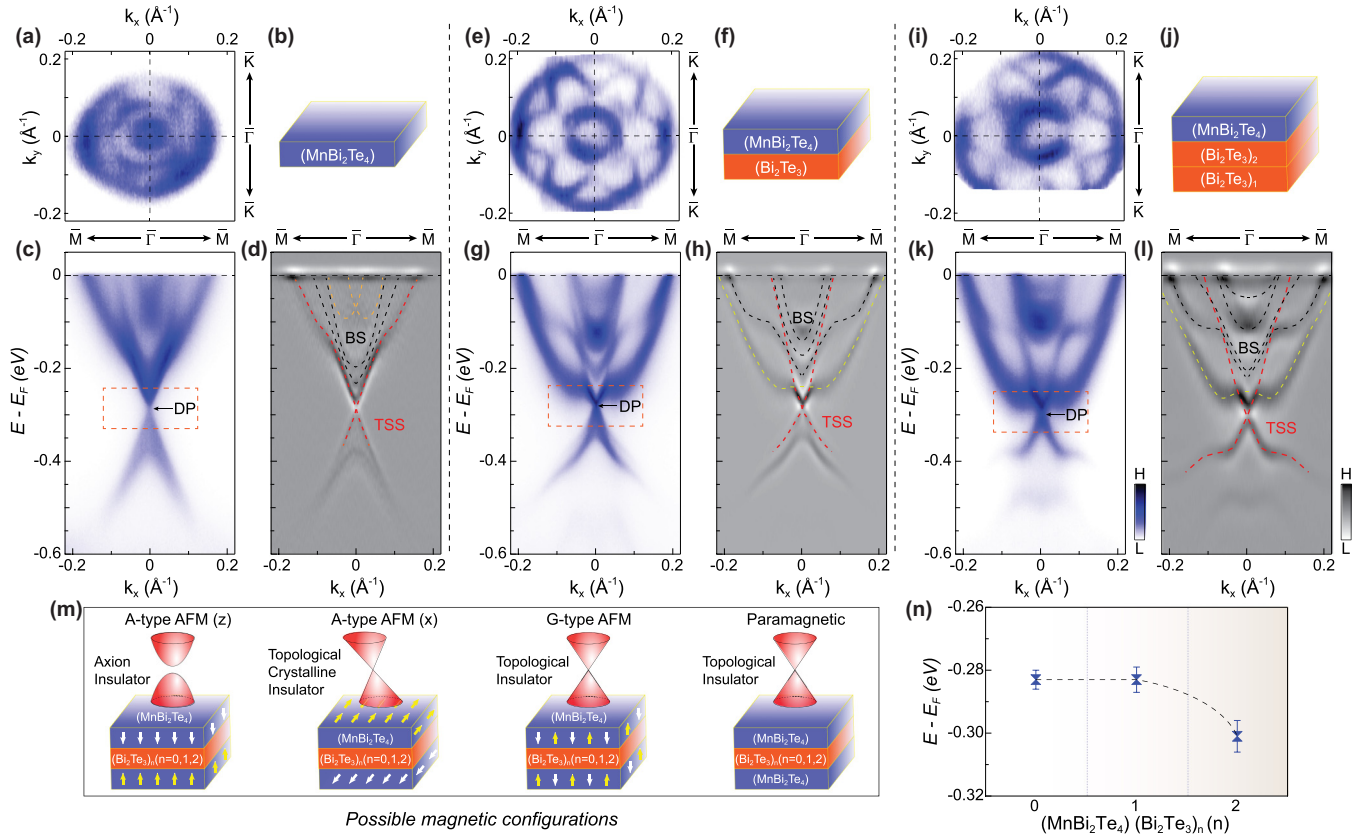

FIG. 3. Electronic structure on the $(MnBi_2Te_4)$ terminated surfaces of $MnBi_2Te_4$, $MnBi_4Te_7$, and $MnBi_6Te_{10}$. (a) Fermi surface, (b) schematic of the crystal building block, (c) band dispersion, and (d) its second derivative image, along the M-Γ-M high-symmetry direction for the $MnBi_2Te_4$ system measured at 10 K. (e)–(h) Same as (a)–(d), but for the $MnBi_4Te_7$ system measured at 7 K. (i)–(l) Same as (a)–(d), but for the $MnBi_6Te_{10}$ system measured at 6 K. The Dirac point (DP) is emphasized by the dashed box and marked by the black arrow in (c), (g), and (k). The topological surface state (TSS) and bulk states (BS) are guided by the red and black dashed lines, respectively [(d), (h), and (l)]. (m) Schematics of different magnetic configurations and the corresponding electronic structures. (n) Energy position of the Dirac point in different systems. The error bars represent the energy uncertainties in the determination of the Dirac point.

materials [marked by the red dashed lines in Figs. 3(d), 3(h), and 3(l)]. Two branches of the dispersion intersect each other at the Dirac point, showing the gapless nature of the TSS. This is in sharp contrast to the earlier expectation of a magnetic surface gap in the order of a hundred meV in both $MnBi_2Te_4$ [11,13,18,30] and $MnBi_4Te_7$ [27,28]. On the contrary, our results are consistent with the recent observation of a gapless TSS in $MnBi_2Te_4$ [21–24] (see Fig. S4 for a detailed analysis of the gapless Dirac state [37]). This universal gapless TSS persists to high temperatures above the magnetic transition temperature of each material system (Fig. S5 [37]), making it an intrinsic property of $(MnBi_2Te_4)$ terminated $(MnBi_2Te_4)_m(Bi_2Te_3)_n$ heterostructures.

After showing the gapless Dirac point, we move to the specific band dispersion of the TSSs (see Fig. S6 for the identification of the TSSs [37]). Different from the Dirac point whose existence is guaranteed by the topological character of the bulk states, the specific band dispersion of the TSSs is always tied to the surface layer itself [33,34]. For example, van der Waals heterostructures with one quintuple layer (QL) Bi_2Te_3 on top of ten QL Bi_2Se_3 (or Sb_2Te_3) give rise to almost the same surface band dispersion as that in the three-dimensional (3D) topological insulator Bi_2Te_3 [34,38]. Surprisingly, different band dispersions of the TSSs are found on the same $(MnBi_2Te_4)$ terminated surface layer in our systems (Fig. 3). First, the band of the TSSs disperses differently between $MnBi_2Te_4$, $MnBi_4Te_7$, and $MnBi_6Te_{10}$ [e.g., different slopes of the band dispersion, marked by the red dashed lines in Figs. 3(d), 3(h), and 3(l)]. Second, the location of the Dirac point moves to a deeper binding energy in $MnBi_6Te_{10}$ compared to that in $MnBi_2Te_4$ and $MnBi_4Te_7$ [Fig. 3(n)]. The same is true for the (Bi_2Te_3) termination, on which different band dispersions of the TSSs are identified (Fig. 4) (see Fig. S7 for the identification of the TSSs [37]). In $MnBi_6Te_{10}$, two distinct topological surface bands are observed on two types of Bi_2Te_3 surface layers, respectively [Figs. 4(a)–4(h)]. These two Bi_2Te_3 surface layers are identical by themselves but are inequivalent by considering different stackings of the layers beneath them [compare Figs. 4(b) and 4(f)]. A (Bi_2Te_3) terminated surface also exists in $MnBi_4Te_7$, which shows a topological surface band different from the above two in $MnBi_6Te_{10}$ [Figs. 4(i)–4(l)]. These results show that the TSSs in $(MnBi_2Te_4)_m(Bi_2Te_3)_n$ heterostructures are sensitive not only to the surface layer, but also to the underlying layers.

Now we discuss the possible origin of the above key observations in $(MnBi_2Te_4)_m(Bi_2Te_3)_n$ heterostructures. First, we need to understand the universal gapless TSS

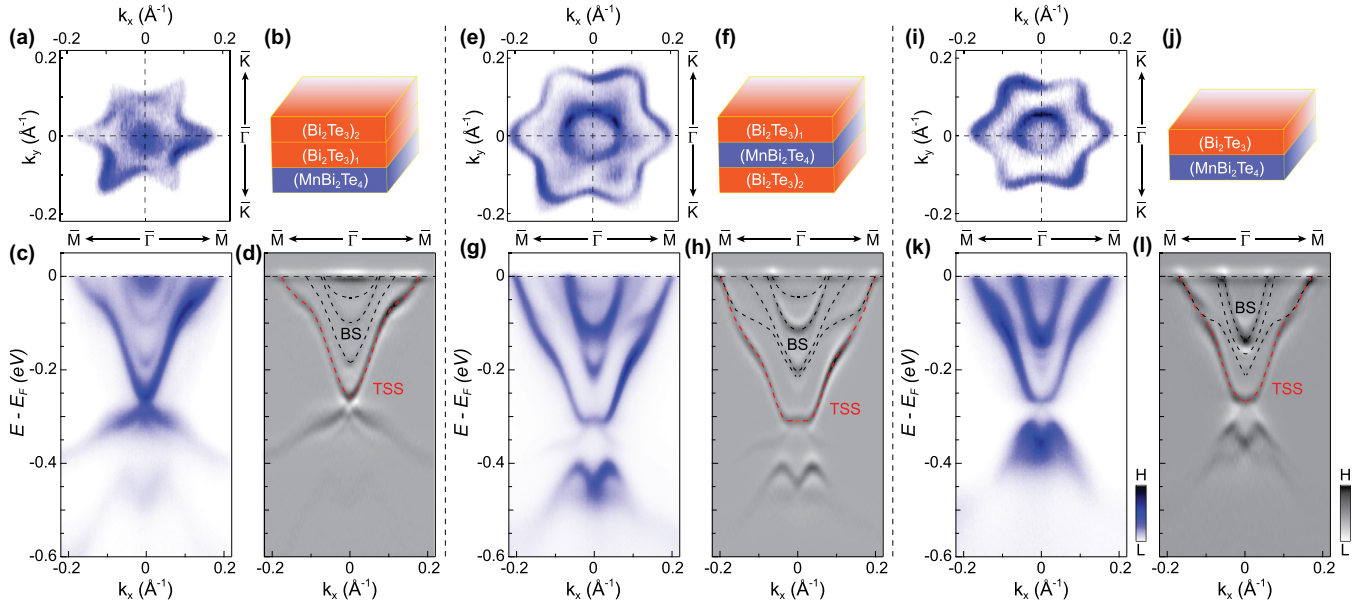

FIG. 4. Electronic structure on the (Bi_2Te_3) terminated surfaces of $MnBi_4Te_7$ and $MnBi_6Te_{10}$. (a) Fermi surface, (c) band dispersion, and (d) its second derivative image, along the M-Γ-M high-symmetry direction for the type-2 (Bi_2Te_3) termination of $MnBi_6Te_{10}$, as illustrated by the schematic in (b). (e)–(h) Same as (a)–(d), but for the type-1 (Bi_2Te_3) termination of $MnBi_6Te_{10}$, as illustrated by the schematic in (f). (i)–(l) Same as (a)–(d), but for the (Bi_2Te_3) termination of $MnBi_4Te_7$, as illustrated by the schematic in (j). The measurements on $MnBi_4Te_7$ ($MnBi_6Te_{10}$) were performed at 7 K (6 K). The topological surface state (TSS) and bulk states (BS) are guided by the red and black dashed lines, respectively [(d), (h), and (l)].

[39]. The magnetic moments in the ground state of $(MnBi_2Te_4)_m(Bi_2Te_3)_n$ are ferromagnetically ordered within a Mn plane along the z direction, but antiferromagnetically coupled between layers [15,40,41]. In theory, this so-called A-type antiferromagnetic order would inevitably induce a sizable magnetic gap in the (0001) surface states, which is incompatible with the gapless TSS observed in our experiment. The universality of the gapless TSS rules out any specific property of the $MnBi_2Te_4$ crystal as the origin. A different strength of the interlayer antiferromagnetic exchange coupling between $MnBi_2Te_4$, $MnBi_4Te_7$, and $MnBi_6Te_{10}$ also makes the interlayer coupling strength less relevant in this connection. One simple explanation involves impurity states, which would potentially fill up the intrinsic magnetic gap. This scenario seems to be consistent with the earlier experimental reports of defects and vacancies [11,13–15]. However, the electron density of states from localized impurities cannot give rise to any band dispersion in the momentum space. Therefore, the impurity scenario cannot explain our experimental observation of a Dirac point at the intersection of two bands. Another possibility is the existence of a trivial surface state in the magnetic gap. However, we have observed a universal Dirac point with different band dispersions in $MnBi_2Te_4$, $MnBi_4Te_7$, and $MnBi_6Te_{10}$, indicating the topological nature of the Dirac-like surface states. The third possibility is the coexistence of multiple short-range magnetic orders (presumably in different domains), such that the global magnetic moment in each layer could be zero. A transport measurement on $MnBi_4Te_7$ does reveal a competition between different magnetic orders at low temperatures, due to the moderate interlayer antiferromagnetic exchange coupling [28]. This scenario can also be naturally extended to $MnBi_6Te_{10}$, which has an even weaker interlayer coupling [28]. However, it contradicts the neutron diffraction measurements on $MnBi_2Te_4$, in which an A-type long-range antiferromagnetic order has been established as the ground state [15]. Therefore, if we assume the same origin for the observed gapless TSS in $(MnBi_2Te_4)_m(Bi_2Te_3)_n$ heterostructures, a more plausible explanation is the change of magnetic configuration in the few top layers of the sample—possibly during the cleaving process. In $MnBi_2Te_4$, several magnetic structures have been suggested to produce a gapless TSS [Fig. 3(m)], including A-type antiferromagnetic order with in-plane magnetic moment, G-type antiferromagnetic order (magnetic moments aligned antiferromagnetically both in plane and between adjacent layers), and disordered magnetic moments (or paramagnetic state) [21]. We have performed density functional theory (DFT) calculations and confirmed that the gapless TSS can also be induced by these magnetic structures in $MnBi_4Te_7$ and $MnBi_6Te_{10}$. While more efforts are needed to pin down the exact magnetic structure near the surface, we find that the calculated bands from the G-type antiferromagnetic order and paramagnetic state exhibit a better agreement with the experimental results comparing to that from the A-type in-plane antiferromagnetic order (see Fig. S8 [37]). Regardless of the exact new state, our results indicate that the magnetic structure of the $(MnBi_2Te_4)_m(Bi_2Te_3)_n$ system may be easily changed, supporting the proposal to realize various topological quantum phases via magnetic tuning [29,35].

Next, we discuss the band dispersions of the TSSs in $(MnBi_2Te_4)_m(Bi_2Te_3)_n$ heterostructures. In topological materials, the gapless nature of the TSSs is determined by

the topological character of the bulk band, but the specific band structure of the TSSs is dominated by the environment near the sample surface [33,34]. This environment is typically determined by the surface layer itself. However, in our measurements, different topological surface band dispersions are observed on nominally the same surface termination, indicating that the surface environment of the $(MnBi_2Te_4)_m(Bi_2Te_3)_n$ is changed by different stackings of the underlying layers. In particular, the underlying magnetic layers of $MnBi_2Te_4$ might have played a key role. First, the band dispersion of the TSS on the (Bi_2Te_3) termination is similar to that of 3D Bi_2Te_3 when the $MnBi_2Te_4$ layer is separated away from the surface by another layer of Bi_2Te_3 [type-2 (Bi_2Te_3) termination of $MnBi_6Te_{10}$; see Figs. 4(a)–4(d)]. This band dispersion is substantially modified when the $MnBi_2Te_4$ layer is located adjacent to the surface [type-1 (Bi_2Te_3) termination of $MnBi_6Te_{10}$; see Figs. 4(e)–4(h)]. Second, the band dispersion of the TSS on the $(MnBi_2Te_4)$ termination is also significantly changed when the coupling between two $MnBi_2Te_4$ layers is reduced by the intercalated Bi_2Te_3 layer(s) (Fig. 3). In this sense, the existence of two building blocks in $(MnBi_2Te_4)_m(Bi_2Te_3)_n$ heterostructures provides a unique tuning knob to manipulate the TSSs without changing the surface of the sample. The direct response between the TSSs and the interlayer coupling also echoes the theoretical proposal to realize various exotic topological phases by different stackings and thicknesses of the $MnBi_2Te_4$ and Bi_2Te_3 layers in this system [29]. It would be instructive to quantitatively investigate how the magnetic layers and interlayer coupling modify the surface environment, as well as whether they are related to the possible change of magnetic configuration in the few top layers of the sample.

In conclusion, we have systematically studied a series of $(MnBi_2Te_4)_m(Bi_2Te_3)_n$ heterostructures with different terminations. A universal gapless TSS is established on the $(MnBi_2Te_4)$ terminated surfaces, which is consistent with a changed magnetic configuration near the surface. The observed topological surface band dispersion is sensitive not only to the surface but also to different stackings of the underlying layers. As such, our findings point to the high tunability of both magnetic and electronic structures of the topological surface states in $(MnBi_2Te_4)_m(Bi_2Te_3)_n$. The switchable magnetic configuration and different combinations of the two building blocks would serve as two natural tuning knobs to realize various topological phases in this system.

We thank Y. Xu and B. Lei for useful discussions. The work at University of Science and Technology of China (USTC) was supported by the USTC start-up fund. The work at ShanghaiTech University was supported by the National Key R&D program of China (Grant No. 2017YFA0305400) and the National Natural Science Foundation of China (Grant No. 11674229). The work at Huazhong University of Science and Technology was supported by the Ministry of Science and Technology of China (No. 2018YFA0307000) and the National Natural Science Foundation of China (No. 11874022).

[1] X.-L. Qi and S.-C. Zhang, Rev. Mod. Phys. **83**, 1057 (2011).
[2] N. Regnault and B. A. Bernevig, Phys. Rev. X **1**, 021014 (2011).
[3] C.-Z. Chang, J. S. Zhang, X. Feng, J. Shen, Z. C. Zhang, M. H. Guo, K. Li, Y. B. Ou, P. Wei, L.-L. Wang, Z.-Q. Ji, Y. Feng, S. H. Ji, X. Chen, J. F. Jia, X. Dai, Z. Fang, S.-C. Zhang, K. He, Y. Y. Wang *et al.*, Science **340**, 167 (2013).
[4] J. Wang, B. Lian, X.-L. Qi, and S.-C. Zhang, Phys. Rev. B **92**, 081107(R) (2015).
[5] E. K. Liu, Y. Sun, N. Kumar, L. Muechler, A. L. Sun, L. Jiao, S.-Y. Yang, D. F. Liu, A. J. Liang, Q. N. Xu, J. Kroder, V. Süß, H. Borrmann, C. Shekhar, Z. S. Wang, C. Y. Xi, W. H. Wang, W. Schnelle, S. Wirth, Y. L. Chen *et al.*, Nat. Phys. **14**, 1125 (2018).
[6] Y. Tokura, K. Yasuda, and A. Tsukazaki, Nat. Rev. Phys. **1**, 126 (2019).
[7] I. Belopolski, K. Manna, D. S. Sanchez, G. Q. Chang, B. Ernst, J. X. Yin, S. S. Zhang, T. Cochran, N. Shumiya, H. Zheng, B. Singh, G. Bian, D. Multer, M. Litskevich, X. T. Zhou, S.-M. Huang, B. K. Wang, T.-R. Chang, S.-Y. Xu, A. Bansil *et al.*, Science **365**, 1278 (2019).
[8] D. F. Liu, A. J. Liang, E. K. Liu, Q. N. Xu, Y. W. Li, C. Chen, D. Pei, W. J. Shi, S. K. Mo, P. Dudin, T. Kim, C. Cacho, G. Li, Y. Sun, L. X. Yang, Z. K. Liu, S. S. P. Parkin, C. Felser, and Y. L. Chen, Science **365**, 1282 (2019).
[9] N. Morali, R. Batabyal, P. K. Nag, E. K. Liu, Q. N. Xu, Y. Sun, B. H. Yan, C. Felser, N. Avraham, and H. Beidenkopf, Science **365**, 1286 (2019).
[10] D. S. Lee, T.-H. Kim, C.-H. Park, C.-Y. Chung, Y. S. Lim, W.-S. Seo, and H.-H. Park, CrystEngComm **15**, 5532 (2013).
[11] M. M. Otrokov, I. I. Klimovskikh, H. Bentmann, D. Estyunin, A. Zeugner, Z. S. Aliev, S. Gaß, A. U. B. Wolter, A. V. Koroleva, A. M. Shikin, M. Blanco-Rey, M. Hoffmann, I. P. Rusinov, A. Yu. Vyazovskaya, S. V. Eremeev, Yu. M. Koroteev, V. M. Kuznetsov, F. Freyse, J. Sánchez-Barriga, I. R. Amiraslanov, M. B. Babanly, N. T. Mamedov, N. A. Abdullayev, V. N. Zverev *et al.*, Nature (London) **576**, 416 (2019).
[12] J. H. Li, Y. Li, S. Q. Du, Z. Wang, B.-L. Gu, S.-C. Zhang, K. He, W. H. Duan, and Y. Xu, Sci. Adv. **5**, eaaw5685 (2019).
[13] A. Zeugner, F. Nietschke, A. U. B. Wolter, S. Gaß, R. C. Vidal, T. R. F. Peixoto, D. Pohl, C. Damm, A. Lubk, R. Hentrich, S. K. Moser, C. Fornari, C. H. Min, S. Schatz, K. Kißner, M. Ünzelmann, M. Kaiser, F. Scaravaggi, B. Rellinghaus, K. Nielsch *et al.*, Chem. Mater. **31**, 2795 (2019).
[14] J. H. Cui, M. Z. Shi, H. H. Wang, F. H. Yu, T. Wu, X. G. Luo, J. J. Ying, and X. H. Chen, Phys. Rev. B **99**, 155125 (2019).
[15] J.-Q. Yan, Q. Zhang, T. Heitmann, Z. Huang, K. Y. Chen, J.-G. Cheng, W. Wu, D. Vaknin, B. C. Sales, and R. J. McQueeney, Phys. Rev. Materials **3**, 064202 (2019).
[16] B. Chen, F. C. Fei, D. Q. Zhang, B. Zhang, W. L. Liu, S. Zhang, P. D. Wang, B. Y. Wei, Y. Zhang, Z. W. Zuo, J. W. Guo, Q. Q. Liu, Z. L. Wang, X. C. Wu, J. Y. Zong, X. D. Xie, W. Chen, Z. Sun, S. C. Wang, Y. Zhang *et al.*, Nat. Commun. **10**, 4469 (2019).
[17] Y. Gong, J. W. Guo, J. H. Li, K. J. Zhu, M. H. Liao, X. Z. Liu, Q. H. Zhang, L. Gu, L. Tang, X. Feng, D. Zhang, W. Li, C. L. Song, L. L. Wang, P. Yu, X. Chen, Y. Y. Wang, H.

Yao, W. H. Duan, Y. Xu *et al.*, Chin. Phys. Lett. **36**, 076801 (2019).

[18] S. H. Lee, Y. L. Zhu, Y. Wang, L. X. Miao, T. Pillsbury, H. M. Yi, S. Kempinger, J. Hu, C. A. Heikes, P. Quarterman, W. Ratcliff, J. A. Borchers, H. D. Zhang, X. L. Ke, D. Graf, N. Alem, C.-Z. Chang, N. Samarth, and Z. Q. Mao, Phys. Rev. Research **1**, 012011(R) (2019).

[19] Y. J. Deng, Y. J. Yu, M. Z. Shi, Z. X. Guo, Z. H. Xu, J. Wang, X. H. Chen, and Y. B. Zhang, Science **367**, 895 (2020).

[20] C. Liu, Y. C. Wang, H. Li, Y. Wu, Y. X. Li, J. H. Li, K. He, Y. Xu, J. S. Zhang, and Y. Y. Wang, Nat. Mater. (2020), doi: 10.1038/s41563-019-0573-3.

[21] Y.-J. Hao, P. F. Liu, Y. Feng, X.-M. Ma, E. F. Schwier, M. Arita, S. Kumar, C. W. Hu, R. Lu, M. Zeng, Y. Wang, Z. Y. Hao, H.-Y. Sun, K. Zhang, J. W. Mei, N. Ni, L. S. Wu, K. Shimada, C. Y. Chen, Q. H. Liu, and C. Liu, Phys. Rev. X **9**, 041038 (2019).

[22] Y. J. Chen, L. X. Xu, J. H. Li, Y. W. Li, H. Y. Wang, C. F. Zhang, H. Li, Y. Wu, A. J. Liang, C. Chen, S. W. Jung, C. Cacho, Y. H. Mao, S. Liu, M. X. Wang, Y. F. Guo, Y. Xu, Z. K. Liu, L. X. Yang, and Y. L. Chen, Phys. Rev. X **9**, 041040 (2019).

[23] H. Li, S.-Y. Gao, S.-F. Duan, Y.-F. Xu, K.-J. Zhu, S.-J. Tian, J.-C. Gao, W.-H. Fan, Z.-C. Rao, J.-R. Huang, J.-J. Li, D.-Y. Yan, Z.-T. Liu, W.-L. Liu, Y.-B. Huang, Y.-L. Li, Y. Liu, G.-B. Zhang, P. Zhang, T. Kondo *et al.*, Phys. Rev. X **9**, 041039 (2019).

[24] P. Swatek, Y. Wu, L.-L. Wang, K. Lee, B. Schrunk, J. Q. Yan, and A. Kaminski, Phys. Rev. B **101**, 161109 (2020).

[25] Z. S. Aliev, I. R. Amiraslanov, D. I. Nasonova, A. V. Shevelkov, N. A. Abdullayev, Z. A. Jahangirli, E. N. Orujlu, M. M. Otrokov, N. T. Mamedov, M. B. Babanly, and E. V. Chulkov, J. Alloys Compd. **789**, 443 (2019).

[26] D. Souchay, M. Nentwig, D. Günther, S. Keilholz, J. de Boor, A. Zeugner, A. Isaeva, M. Ruck, A. U. B. Wolter, B. Büchner, and O. Oeckler, J. Mater. Chem. C **7**, 9939 (2019).

[27] C. W. Hu, K. N. Gordon, P. F. Liu, J. Y. Liu, X. Q. Zhou, P. P. Hao, D. Narayan, E. Emmanouilidou, H. Y. Sun, Y. T. Liu, H. Brawer, A. P. Ramirez, L. Ding, H. B. Cao, Q. H. Liu, D. Dessau, and N. Ni, Nat. Commun. **11**, 97 (2020).

[28] J. Z. Wu, F. C. Liu, M. Sasase, K. Ienaga, Y. Obata, R. Yukawa, K. Horiba, H. Kumigashira, S. Okuma, T. Inoshita, and H. Hosono, Sci. Adv. **5**, eaax9989 (2019).

[29] H. Sun, B. Xia, Z. Chen, Y. Zhang, P. Liu, Q. Yao, H. Tang, Y. Zhao, H. Xu, and Q. Liu, Phys. Rev. Lett. **123**, 096401 (2019).

[30] R. C. Vidal, H. Bentmann, T. R. F. Peixoto, A. Zeugner, S. Moser, C.-H. Min, S. Schatz, K. Kißner, M. Ünzelmann, C. I. Fornari, H. B. Vasili, M. Valvidares, K. Sakamoto, D. Mondal, J. Fujii, I. Vobornik, S. Jung, C. Cacho, T. K. Kim, R. J. Koch *et al.*, Phys. Rev. B **100**, 121104(R) (2019).

[31] M. M. Otrokov, I. P. Rusinov, M. Blanco-Rey, M. Hoffmann, A. Yu. Vyazovskaya, S. V. Eremeev, A. Ernst, P. M. Echenique, A. Arnau, and E. V. Chulkov, Phys. Rev. Lett. **122**, 107202 (2019).

[32] D. Q. Zhang, M. J. Shi, T. S. Zhu, D. Y. Xing, H. J. Zhang, and J. Wang, Phys. Rev. Lett. **122**, 206401 (2019).

[33] Y. F. Zhao, C. Z. Chang, Y. Jiang, A. DaSilva, Y. Sun, H. C. Wang, Y. Xing, Y. Wang, K. He, X. C. Ma, Q.-K. Xue, and J. Wang, Sci. Rep. **3**, 3060 (2013).

[34] C.-Z. Chang, P. Z. Tang, X. Feng, K. Li, X.-C. Ma, W. H. Duan, K. He, and Q.-K. Xue, Phys. Rev. Lett. **115**, 136801 (2015).

[35] J. H. Li, C. Wang, Z. T. Zhang, B.-L. Gu, W. H. Duan, and Y. Xu, Phys. Rev. B **100**, 121103(R) (2019).

[36] M. Z. Shi, B. Lei, C. S. Zhu, D. H. Ma, J. H. Cui, Z. L. Sun, J. J. Ying, and X. H. Chen, Phys. Rev. B **100**, 155144 (2019).

[37] See Supplemental Material at http://link.aps.org/supplemental/10.1103/PhysRevB.101.161113 for sample characterizations, identifications of the electronic structures on different terminations, first principles calculations, and other supporting information.

[38] Y. L. Chen, J. G. Analytis, J.-H. Chu, Z. K. Liu, S.-K. Mo, X. L. Qi, H. J. Zhang, D. H. Lu, X. Dai, Z. Fang, S. C. Zhang, I. R. Fisher, Z. Hussain, and Z.-X. Shen, Science **325**, 178 (2009).

[39] Recently, we became aware that a gapless topological surface state in $MnBi_4Te_7$ was also reported in Refs. [23,42].

[40] L. Ding, C. W. Hu, F. Ye, E. Feng, N. Ni, and H. B. Cao, Phys. Rev. B **101**, 020412(R) (2020).

[41] J.-Q. Yan, Y. H. Liu, D. Parker, M. A. McGuire, and B. C. Sales, arXiv:1910.06273.

[42] L. X. Xu, Y. H. Mao, H. Y. Wang, J. H. Li, Y. J. Chen, Y. Y. Y. Xia, Y. W. Li, J. Zhang, H. J. Zheng, K. Huang, C. F. Zhang, S. T. Cui, A. J. Liang, W. Xia, H. Su, S. W. Jung, C. Cacho, M. X. Wang, G. Li, Y. Xu *et al.*, arXiv:1910.11014.